

SYNTHETIC APERTURE RADAR FOR ASSESSING LAND DEGRADATION IN A SALT MINING AREA – OCNELE MARI CASE-STUDY

VIOLETA POENARU*, ALEXANDRU BADEA**, SORIN MIHAI CÎMPEANU***, IULIA DANA NEGULA****

Key-words: Ocnele Mari, land degradation, geomorphologic conditions, Synthetic Aperture Radar, SAR Interferometry, SAR polarimetry.

Abstract. Human activities through anthropogenic changes had negative impacts not only on land cover, but on many aspects of local, regional and global environments, including climate, biodiversity, soil condition and sediment flow. Remote sensing imagery with its useful qualitative and quantitative observations acquired repetitively and with large spatial coverage, offers opportunity for early detection and warning of land degradation risk. This paper investigates the Synthetic Aperture Radar techniques potential to assess land degradation in a salt mining area affected by subsidence phenomena. Based on backscattering temporal variability of SAR data and coherence, we propose to analyze a multi-temporal RADARSAT2 data acquired in interferometric mode by applying SAR interferometry, SAR polarimetry and SAR change detection approaches.

1. INTRODUCTION

Human activities through anthropogenic changes had negative impacts not only on land cover but on many aspects of local, regional and global environments, including climate, biodiversity, soil condition and sediment flow. Land degradation processes which imply soil degradation and accelerated erosion, reduction of the quantity and diversity of natural vegetation are widely spread in Vâlcea County (Poenaru *et al.*, 2011, Poenaru *et al.*, 2012).

Remote sensing imagery with its useful qualitative and quantitative observations acquired repetitively and with a large spatial coverage offers opportunity for early detection and warning of land degradation risk. Synthetic Aperture Radar (SAR) images present special operational utilities and detection capabilities and could be used to updating maps and monitoring dynamic land-use processes over time. The objective of this paper is to investigate land degradation by SAR techniques such as: SAR interferometry (InSAR), polarimetric SAR processing and analysis (PolSAR) and noncoherent analysis. These techniques use both phase and amplitude information to estimate land degradation and to detect changes in backscattered signal response.

As SAR is a coherent image system, Interferometric SAR systems record both amplitude and phase of the backscattered echoes acquired with slightly different viewing angle (interferometric pair), their phase differences (interferometric fringes) being exploited for Digital Elevation Model (DEM) generation and terrain changes monitoring (landslides and subsidence) (Zebker and Goldstain, 1986, Werner *et al.*, 1993). Interferometric fringes are observed where image coherence prevails and show a 2π change in the wave phase, assigning it a color scale (blue-green-yellow-red) or grey scale. An area is coherent if surface characteristics remain unchanged in all images. The land surfaces covered with

* Researcher, Romanian Space Agency, 21-25 Mendeleev Av., 010362, District 1, Bucharest, Romania & University of Agronomic Science and Veterinary Medicine, Bvd. Mărăști, no. 59, 011464, District 1, Bucharest, Romania, violeta.poenaru@rosa.ro.

** Professor, Romanian Space Agency, 21–25 Mendeleev Av., 010362, District 1, Bucharest, Romania, alexandru.badea@rosa.ro.

*** Professor, University of Agronomic Science and Veterinary Medicine, Bvd. Mărăști, no. 59, Bucuresti, 011464, District 1, Bucharest, Romania, sorin.cimpeanu@usamv.ro.

**** Researcher, Romanian Space Agency, 21–25 Mendeleev Av., 010362, District 1, Bucharest, Romania, iulia.dana@rosa.ro.

vegetation (forest, agricultural land) introduce noise in the radar signal (decorrelation) and no information is obtainable. There are several sources which contribute to the decorrelation (Zebker and Villasenor, 1992, Hanssen, 2001) such as: spatial (the distance between the satellite tracks during acquisitions, namely baseline), temporal (time between acquisitions), thermal (system noise), Doppler Centroid and volumetric (radar penetration through the scattering medium).

The interferometric phase, expressed as in eq. 1, is affected by the distance between antenna and ground pixel, surface topography, satellite orbits, the dielectric properties of the ground surface, atmosphere and system noise.

$$\Delta\phi = \Delta\phi_{topo} + \Delta\phi_{defo} + \Delta\phi_{atm} + \Delta\phi_{pixel} + \Delta\phi_{noise} + \Delta\phi_{error} \quad (1)$$

Where:

$\Delta\phi_{topo}$ is the surface topography, corrected by applying a DEM;

$\Delta\phi_{defo}$ is the line-of-sight (LOS) displacement (surface displacement in the direction between the satellite and ground pixel);

$\Delta\phi_{atm}$ represents the atmospheric artifacts which can be reduced by generation and combination of multiple interferograms, a technique known as stacking;

$\Delta\phi_{pixel}$ represents changes in the reflectivity of the observed pixel (soil moisture changes);

$\Delta\phi_{noise}$ is the phase noise term which can be reduced by using adaptive filtering and multi-look techniques

$\Delta\phi_{error}$ are errors associated with phase unwrapping, uncertainties in the knowledge of the platform position and baseline.

InSAR estimate deformation in the LOS direction of the radar beam implies that only one component of the deformation can be measured in an individual interferogram. By using multiple satellite passes with different geometries (Wright *et al.*, 2004), it is possible to decompose InSAR LOS measurements into north, east, south and west components. For a single multitemporal imaging geometry, some authors (Kratzsch, 1983, Samieie-Esfahany *et al.*, 2009) suggest that the horizontal displacement is proportional to the tilt and can be neglected so that the vertical deformation component is derived.

InSAR principle method can be used in differential interferometry (DInSAR) by combining a pair of short baseline SAR images enough separated in time to generate the associated interferogram so that the interferometric phase variation is removed from underlying topography. The applicability of this technique was demonstrated in many studies regarding detection of earthquake displacement (Massonet *et al.*, 1993), volcano deformation (Massonet *et al.*, 1995), monitoring of ice sheet motions (Goldstein *et al.*, 1993), measuring ocean surface currents (Goldstein and Zebker, 1987, Goldstein *et al.*, 1989) and land subsidence (Strozzi and Wegmuller, 1999, Ferretti *et al.*, 2000). An advanced DInSAR method uses stable point network and coherent pixel technique to distinguish regional from local deformation processes (Herrera *et al.*, 2009).

Persistent scatterer interferometry (PSInSAR) is based on differential interferometry and identifies pixels that are coherent over long time-intervals enabling detection of Earth surface deformations at the millimeter level (Ferretti *et al.*, 2000, Ferretti *et al.*, 2001). The main advantages are filtering out of the atmospheric artefacts and elimination of the temporal and geometrical decorrelation. One of the limitation issues is a loss of data continuity because the data are a set of points with a density that depends on the form and coverage of the surface. These coherent radar targets are abundant in urban areas and sparse in vegetated and hilly areas.

SAR polarimetry provides more target properties information than single polarization SAR system. The interactions between the electromagnetic waves and the observed targets depend on

frequency, polarization and incident angle of the SAR sensor, but also on the surface properties of the targets such as scattering behavior, geometrical structure and dielectric properties. The applications of this technique include: land use / land cover mapping (Chen *et al.*, 2013, Duy, N.B. *et al.*, 2012, Zhixin Qi *et al.*, 2012), change detection (Kersten, P.R. *et al.*, 2005, Meng Liu *et al.*, 2012, Ghanbari, M. *et al.*, 2014), hazard monitoring and damage assessment (Czuchlewski, K.R. *et al.*, 2005, Cao, Yun-gang *et al.*, 2008), surface geophysical parameters retrieval (surface roughness and soil moisture content) (Yunjin Kim and Jacob J. Van Zyl, 2009, Shui Gao *et al.*, 2013), biomass and forest height estimation (Luo, H.M. *et al.*, 2010, Treuhaft, R.N. and Siquira, P., 2000).

Based on advantages of the synthetic aperture radar techniques, this paper assesses land degradation in the Ocnele Mari salt mining area with RADARSAT2 dual polarized data acquired in the SOAR-16605 scientific proposal framework covering the July to December 2014 period.

2. STUDY AREA DESCRIPTION AND DATA

The Ocnele Mari salt mining area, located in the Central-Southern part of Romania, in Vâlcea SubCarpathian area (Fig. 1), surrounded by hills of 400–600 m altitude, is one of the older human settlement in the Oltenia region. The salt deposit is stratiform with a lenticular shape that appears as a cushion developed in the east-west direction (about 7.5 km) with a width of 2.5 km (Băltesanu *et al.*, 2006).

Many studies have been conducted in the salt mining area for subsidence and seismic activities monitoring (Zamfirescu *et al.*, 2003; Zamfirescu. *et al.*, 2009; Trifu and Shumila, 2010). These phenomena are favored by uncontrolled exploitation of the salt deposit which led to the enlargement of underground voids and also to mining-induced subsidence of the surface. The rocks forming in the region situated above the salt cushion have very low mechanical resistance and height inter-granular fissured permeability so that the hill slopes are affected by landslides which are reactivated periodically (Fig. 2).

As the result of the implementation of the strategic plan regarding safe exploitation and rehabilitation of the salt mining area adopted in 2007, degradation phenomena decreased in intensity

A set of 6 Fine dual polarized RADARSAT-2 complex data acquired between July and December 2014 were used in this study. The SAR images have VV, VH and HH, HV polarization, a resolution of 5m x 5m and an incidence angle of 36°. The multi-temporal information was considered in this work to observe the changes in backscattering coefficient which are relevant in land use/land cover monitoring. LULC classes in the Ocnele Mari area can be summarized into six categories: urban/built-up, deciduous, fruit-tree, pastures, complex cultivation and agriculture with natural vegetation.

For processing and validation purposes, a Digital Elevation Model and a thematic mapper image acquired by Landsat 8 OLI satellite were used.

3. RESULTS AND DISCUSSIONS

InSAR and DinSAR techniques were applied. Four interferometric pairs (Table 1) have been processed to generate coherence images and deformation maps. From these image pairs were chosen, those with short perpendicular baseline to minimize any possible registration error and for easily phase unwrapping. As a rule, interferograms with short baseline are exploited to unwrapping interferograms with high baseline (> 300 m).

Interferometric processing steps consisted in:

1. *Image registration* that means the slave image is resampled to the master dimension;
2. *Interferogram generation* that requires pixel-by pixel computation of the Hermitian product (complex value of first image with complex conjugate value of the second image) of two coregistered images;
3. *Interferogram flattening* in which the reference phase due to earth curvature is subtracting;

4. *Topographical phase removal;*

5. *Coherence estimation and interferogram filtering.* Correlations between coregistrated images are computed: built-up area has high correlation (value to 1) while vegetation coverage introduce decorrelation (value to 0). A Goldstein filter was applied to the interferogram to reduce noise introduced by vegetation and to improve the signal-to-noise ratio (Goldstein *et al.*, 1988).

6. *Phase unwrapping* is the most important processing step because the absolute phase is recovered from the wrapped phase by removing of the 2π ambiguity. We applied minimum cost flow algorithm which enables to obtain better results for large areas of low coherence. Therefore the coherence was set to 0.25, all pixels with coherence below this threshold being masked out.

7. *Phase to displacement conversion and geocoding.* Each interferometric fringe corresponds to half wavelength of displacement along the SAR viewing direction. Thus the phase values are converted to displacement and geocoded onto a map projection (in this case WGS84, geographical coordinates).

The results are shown in Fig. 3 and Fig. 4. The Ocele Mari salt mining area deformation maps yield -1.5 cm to 2.5 cm land degradation for VV polarization and -0.1 cm to 1.9 cm land degradation for HH polarization which confirm the previous results retrieved from TerraSar-X data. In these estimations the atmospheric phase contribution cannot be removed so that the interferograms could be affected by the atmospheric effects. Moreover, the pixel brightness induced by surface soil moisture could influence these estimations.

Table 1

Interferogram image pairs characteristics

Image pair	Polarization	Perpendicular Baseline (m)	Height ambiguity (m)	Displacement ambiguity (m)	Temporal baseline (days)
02.07.2014–26.07.2014	VV	-2.96	5457.2	0.028	24
26.07.2014–19.08.2014	VV	-107.42	150.213	0.028	24
19.08.2014–12.09.2014	VV	-90.62	178.06	0.028	24
23.11.2014–17.12.2014	HH	-17.88	902.26	0.028	24

A multi-temporal analysis was performed to assess land use/ land cover changes. Processing tasks include multilooking, coregistration, despeckling and terrain correction. Backscattering coefficient of different land-use classes were analysed using the ground thruth point (Fig. 5). RADARSAT 2 data showed the clear discrimination of forest, orchards, agricultural area, build-up, barren and water bodies.

Change detection statistics to identify the type and extent of changes that have taken place in Ocele Mari salt mining area in the summer of 2014 was applied. We look for increasing and decreasing in brightness because an increase in brightness might be a result of an increase in soil or canopy moisture. The result shown in Figure 6 confirms optical imagery: changes in soil moisture and SAR imaging geometry (i.e. foreshortening and layover).

In order to monitor vegetation coverage extent, multi-temporal polarimetric analysis was applied on SAR data. The RGB composites using the channel information VV, VH and HV, HH are illustrated in Fig. 7. Signatures of built-up, water body, forest and agricultural area are used to support a supervised classification in the study area. Entropy (H), anisotropy (A) and alpha angle (α) are extracted from polarimetric SAR data in order to obtain the dominant scattering mechanism and to classify land-use classes (Fig. 8). The entropy provides information on the scattering degree of randomness, while alpha parameter indicates the dominant scattering: single or double bounce scattering over anisotropic media.

The H- α classification plane is sub-divided in 8 basic zone characteristic of different scattering behaviours. The scattering mechanism of each pixel is identified by comparing its entropy and α parameters to fixed thresholds. The different class boundaries in the H- α plane are determined so as to discriminate surface reflection (8, 5), volume diffusion (7, 4, 2) and double bounce reflection (6, 3, 1) along the α axis and low (our case), medium and high degree of randomness along the entropy axis (Cloude, S.R. and Pottier, E., 1997). In the unsupervised classification results (Fig. 10) are observed that

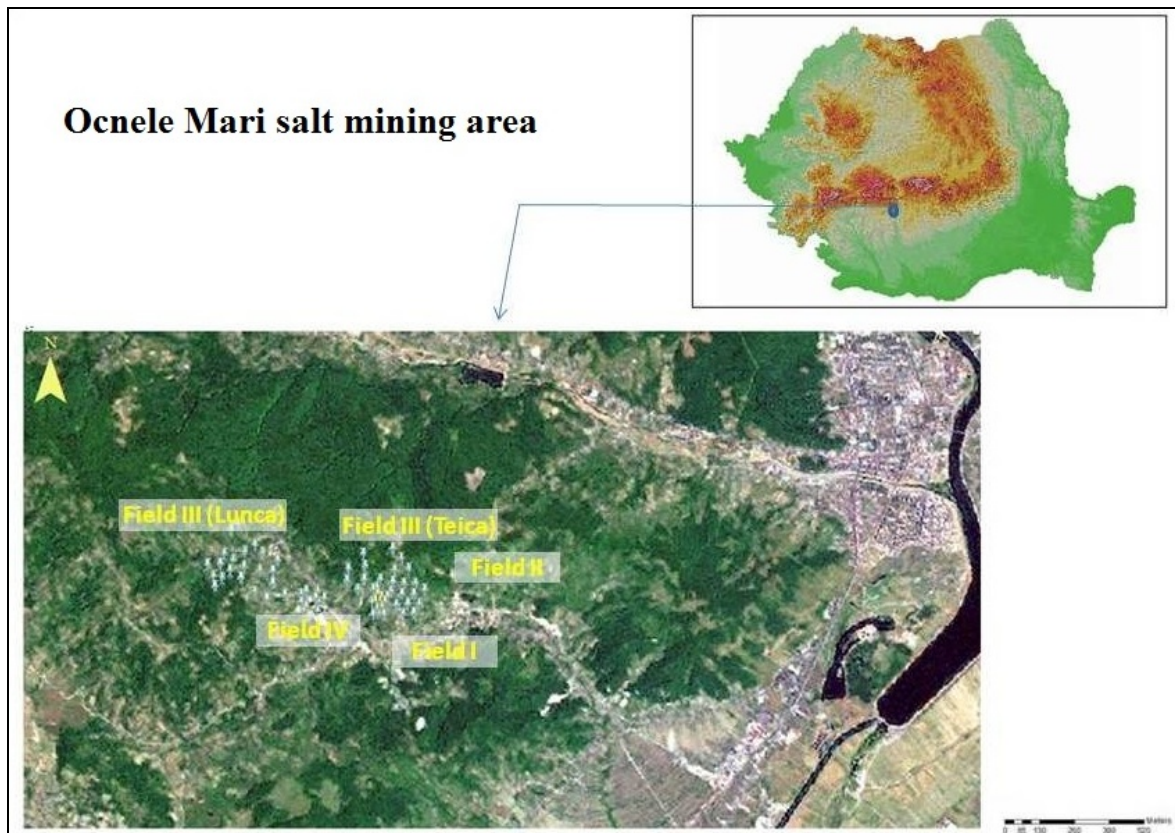


Fig. 1 – Geographic map of the Ocnele Mari salt mining area (courtesy SpotImage 2007). so that the study area became relatively stable in time (-2, -4 mm/yr subsidence) (Poenu, 2013).

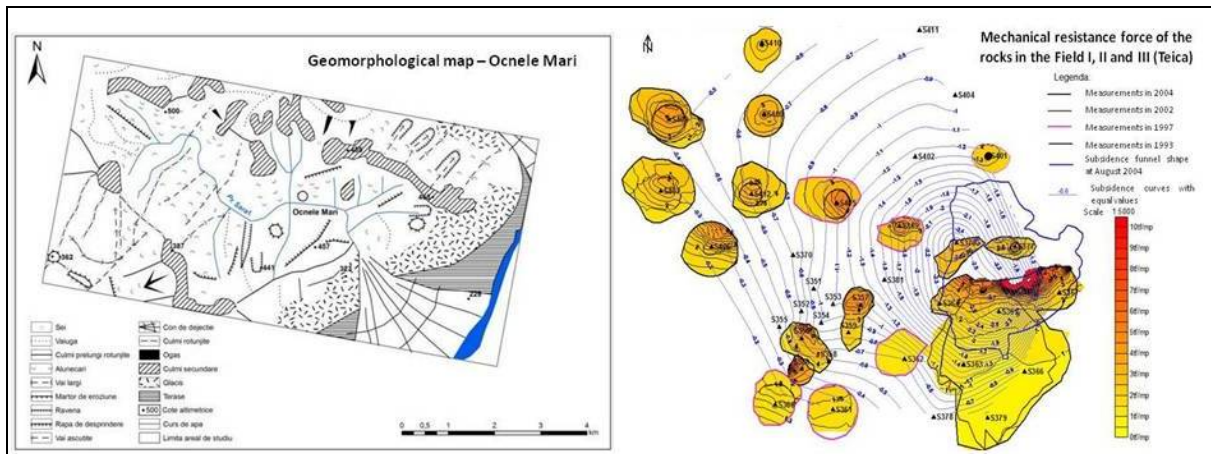


Fig. 2 – Geomorphological map and subsidence induced by mechanical resistance force of the rock in salt mining area (scale 1: 5000) (Zamfirescu et al., 2010).

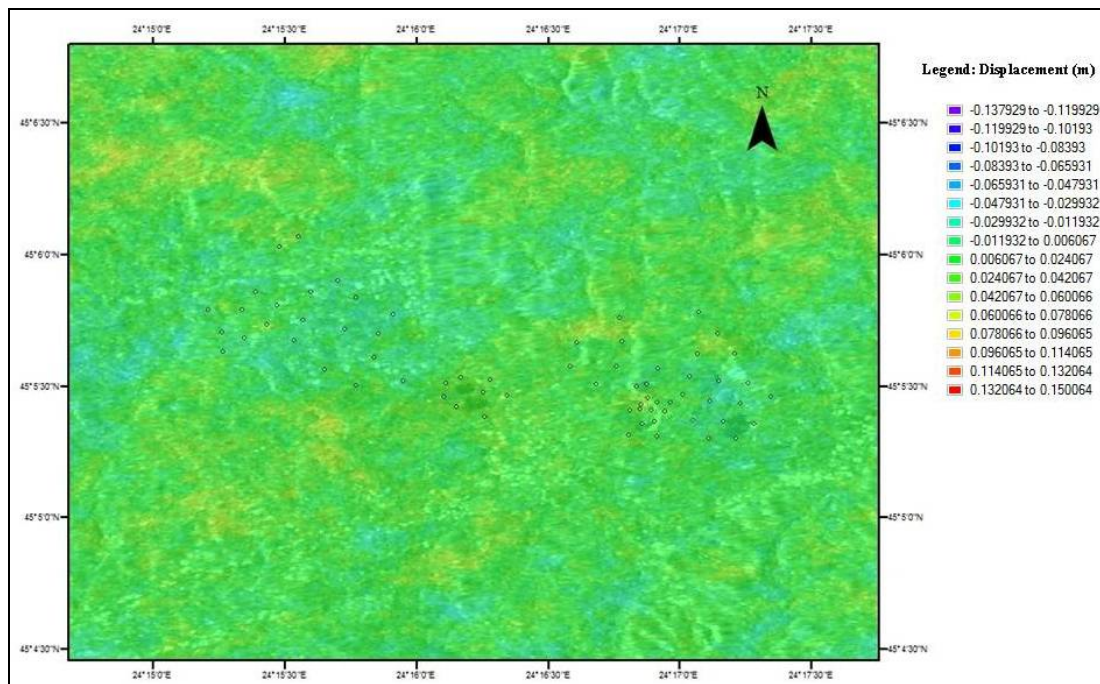


Fig. 3 – Displacement map estimated from 02.07 – 26.07.2014 image pair (VV polarization). RADARSAT 2 data acquired on 02.07.2014 are chosen as background image on which probes vector layer is overlapped. (RADARSAT-2 Data and Products© MacDonald, Dettwiler and Associates LTD (2014) - All right reserved. RADARSAT is an official trademark of the Canadian Space Agency).

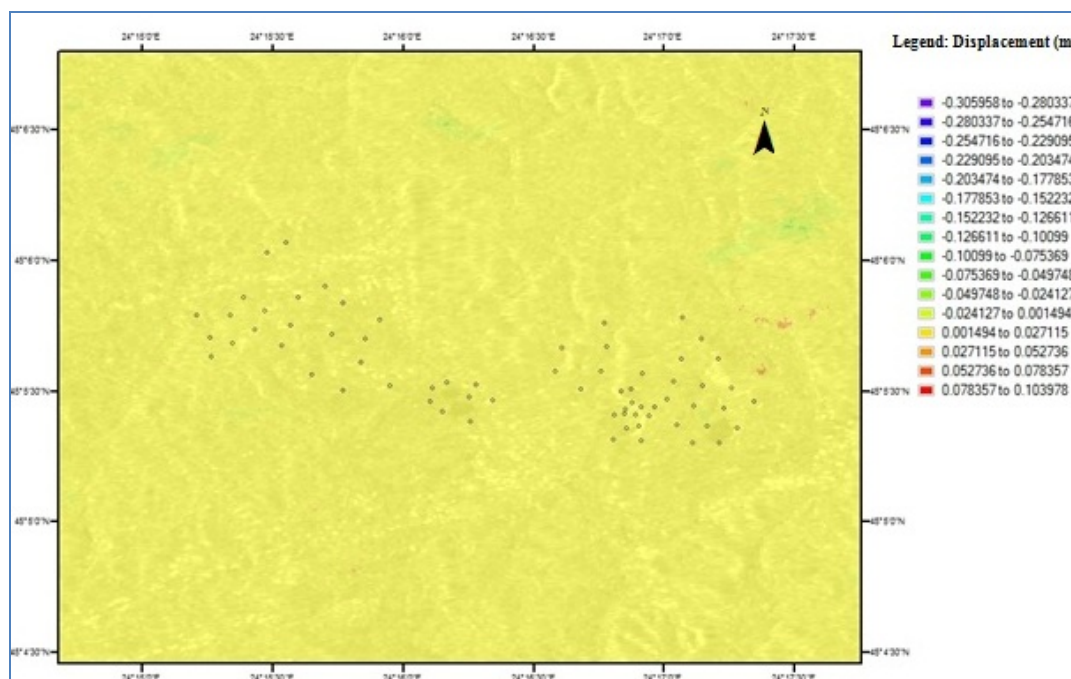


Fig. 4 – Displacement map estimated from 23.11 – 17.12.2014 image pair (HH polarization). RADARSAT 2 data acquired on 23.11.2014 are chosen as background image on which probes vector layer is overlapped. (RADARSAT-2 Data and Products© MacDonald, Dettwiler and Associates LTD (2014) - All right reserved. RADARSAT is an official trademark of the Canadian Space Agency).

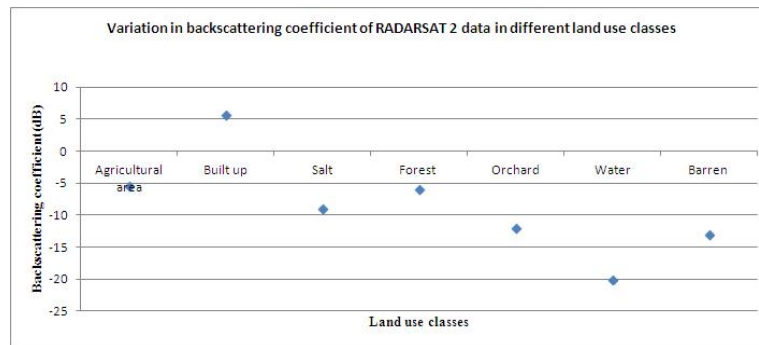


Fig. 5 – Variation of backscattering coefficient of RADARSAT 2 data in different land use classes.

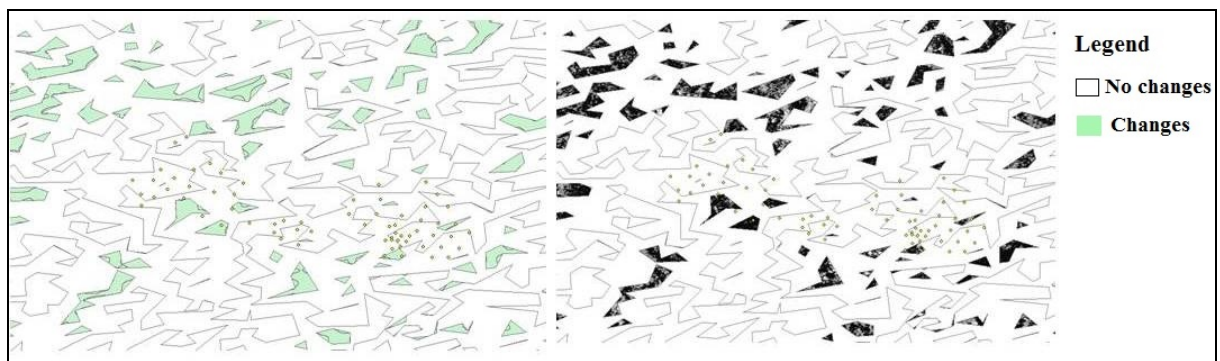


Fig. 6 – Amplitude change detection differences of backscattering coefficients.

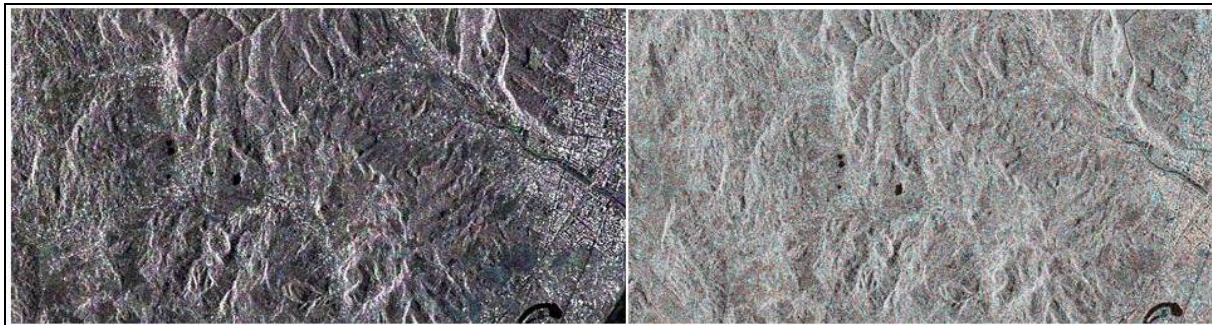


Fig. 7 – Multitemporal VV polarization SAR RGB composite (left) and polarimetric false colour composite (HH, HV, HH-HV). (RADARSAT-2 Data and Products© MacDonald, Dettwiler and Associates LTD (2014) - All right reserved. RADARSAT is an official trademark of the Canadian Space Agency).

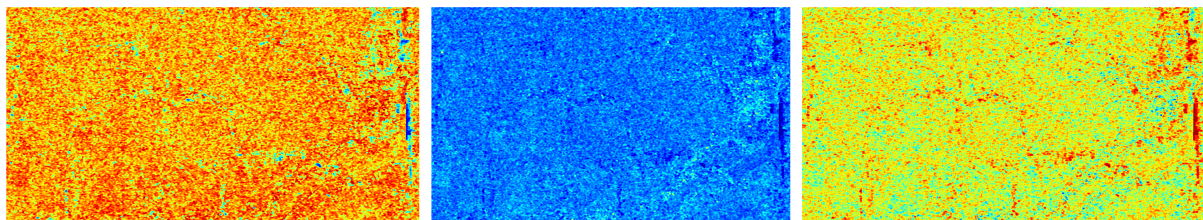


Fig. 8 – Polarimetric decomposition main parameters: *Left*: Entropy; *Middle*: Alpha angle and *Right*: Anisotropy. Scattering over the water body is characterized by a low degree of randomness. The mixing of different scattering mechanism over built-up and agricultural areas results in intermediate entropy values. On the forested areas (red colour) the scattering process is random.

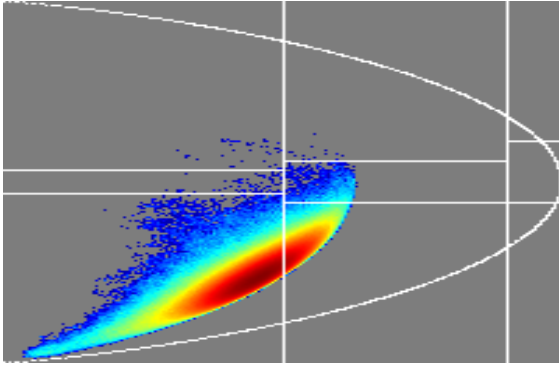


Fig. 9 – Polarimetric data occurrence in the H- α plane

(RADARSAT-2 Data and Products© MacDonalD, Dettwiler and Associates LTD (2014) - All right reserved.
RADARSAT is an official trademark of the Canadian Space Agency).

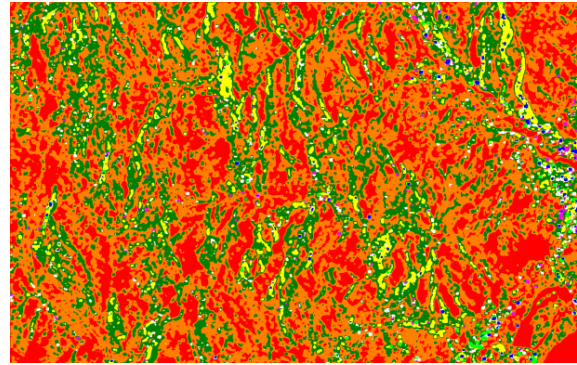


Fig. 10 – Unsupervised scattering mechanism.

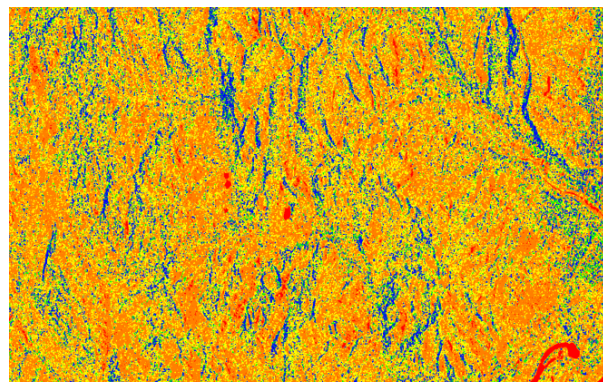
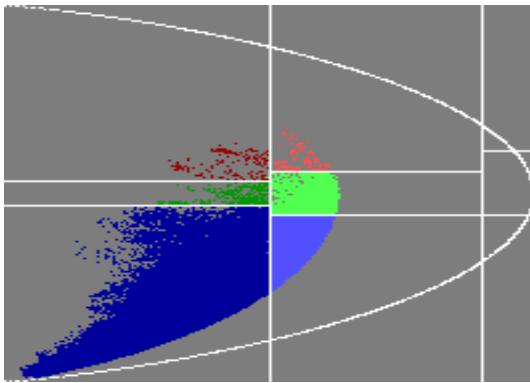


Fig. 11 – Wishart H-A- α segmentation results: *Left* - H- α segmented plane; *Right*: Classification. (RADARSAT-2 Data and Products© MacDonalD, Dettwiler and Associates LTD (2014) - All right reserved. RADARSAT is an official trademark of the Canadian Space Agency).

Wishart segmentation permits to identify the type of the scattering mechanism. Layover effects induced by SAR geometry imaging mode are characterized as surface scattering. Scattering over forested areas is dominated by volume diffusion, while urban areas are mainly characterized by double bounce scattering. It should be noted that the volume diffusion and double bounce scattering are overestimated in this classification because data distribution in the $H-\alpha$ plane does not distinguish natural clusters belonging to a single scattering mechanism class. Therefore, the supervised Wishart segmentation algorithm (maximum likelihood classifier) based on segmentation thresholds was applied to multi-temporal data. An important improvement in the segmentation accuracy can be observed in the image presented in Fig. 11 and Table 2. The main kinds of natural media are clearly discriminated by the segmentation scheme. The Wishart maximum likelihood classifier modifies the decision boundaries in an adaptive way to better fit the natural distribution of the scattering mechanism and takes into account information related to the backscattered intensity.

Table 2

Colour assignment for classification result (see Fig. 11)

Class	Colour	Land use
1	Red	Water body
2	Blue	SAR layover
3	Orange	Vegetation coverage
4	Yellow	Barren soil
5	Green	Urban area

The classification result is affected by SAR geometry effects and topography that induce a relative mixture in the scattering mechanism. If the number of classes is set on vegetation types then they cannot be separable using Wishart classifier. It is therefore important to carefully select the number of classes or take the topography and SAR geometry configuration into account for class interpretation.

4. CONCLUSIONS

This study investigates the Synthetic Aperture Radar techniques potential to assess land degradation in a salt mining area affected by subsidence phenomena. DInSAR technique is applied for land deformation estimation. The results confirm leveling measurement trends of decreasing in subsidence rate but can be influenced by atmospheric artifacts and soil moisture content.

The PolSAR and SAR multitemporal analyses were performed to assess land use/ land cover changes. Change detection reveals an increase of brightness due to soil moisture and layover effects.

The Wishart classifier is versatile for the classification of multi-temporal polarimetric SAR data. The classification accuracy is improved significantly if the Wishart classifier is applied to the multi-temporal dual polarization datasets instead of applying it to one datum of dual polarization dataset. Topography and SAR geometry affect the classification results so the Wishart classifier is recommended for land cover mapping using multi-temporal RADARSAT 2 data.

Acknowledgements

Radarsat-2 imagery was acquired in the joint ESA-CSA SOAR Europe-16605 scientific proposal framework. The paper was done under the frame of European Social Fund, Human Resources Development Operational Programme 2007–2013, project no. POSDRU/159/1.5/S/132765 and with the support of Romanian Space Agency by MEN-UEFISCDI, Program Partnerships, Projects PN-II no 171/2013.

REFERENCES

- Bălteanu, D., Enciu, P. & Deak, G. (2006), *A large scale collapse in the Ocnele Mari salt mine field, Getic Subcarpathians, Romania*, *Studia Geomorfologica Carpatho – Balcanica*, **XL**, pp. 119–126.
- CAO Yun-Gang, YAN Li-Juan & ZHENG Ze-Zhong (2008), *Extraction of information on geology hazard from multi-polarization SAR images*, *The International Archives of the Photogrammetry, Remote Sensing and Spatial Information Sciences*. Vol. **XXXVII**. Part *B4*. Beijing 2008.
- Cloude S.R. and E. Pottier (1997), *An Entropy-Based Classification Scheme for Land Applications of Polarimetric SAR*, *IEEE Trans GRS*, vol. **35**(1), pp. 68–78.
- Czuchlewski, K.R., Weissel, J.K. & Jong-Sen Lee, (2005), *New methods for landslide identification and mapping using SAR polarimetry obtained during the PacRim 2000 mission in Taiwan*, *Geoscience and Remote Sensing Symposium*, 2005. IGARSS '05. Proceedings. 2005 IEEE International, vol. **3**, no., pp. 2086–2089, 25–29 July 2005.
- Ferretti, A., Prati C. & Rocca F. (2001) *Permanent scatterers in SAR interferometry*. *IEEE Transactions on Geoscience and Remote Sensing*, **39**(1), pp. 8–20.
- Ferretti, A., Prati C. & Rocca F. (2000), *Nonlinear subsidence rate estimation using the Permanent Scatterers in differential SAR interferometry*, *IEEE Transactions on Geoscience and Remote Sensing*, **38**(5), pp. 2202–2012.
- Ghanbari, M., Akbari, V., Abkar, A. A., Sahebi, M. R. & Liu, M. (2014), *A robust change detector for multilook polarimetric Synthetic Aperture Radar data*, *International Archives of the Photogrammetry, Remote Sensing & S*;11/15/2014, Vol. **40–2/W3**, p. 127.
- Goldstein, R. M., Barnett, T. P. & Zebker, H. A., (1989), *Remote sensing of ocean currents*, *Science*, **246**, pp. 1282–1285.
- Goldstein, R. M., Zebker, H. A., and Werner, C. L., (1988), *Satellite radar interferometry: Two-dimensional phase unwrapping*. *Radio Sci.*, **23**, pp. 713–720.
- Goldstein, R.M. & Zebker, H.A., (1987), *Interferometric RADAR Measurement of Ocean Surface Currents*, *Nature* **328** (6132): 707. doi:10.1038/328707.
- Goldstein, R.M., Englehardt, H., Kamb, B. & Frolich, R.M. (1993), *Satellite radar interferometry for monitoring ice sheet motion: application to an Antarctic ice stream*. *Science*, **262**, pp. 1525–1530.
- Hanssen, R.F. (2001), *Radar Interferometry: Data Interpretation and Error Analysis*, Kluwer Academic Publishers, Dordrecht, The Netherlands.
- Herrera, G., Tomás, R., López-Sánchez, J.M., Delgado, J., Vicente, F., Mulas, J., Cooksley, G., Sánchez, M., Duro, J., Arnaud, A., Blanco, P., Duque, S., Mallorquí, J.J., Vega-Panizo, R. & Monserrat, O. (2009), *Validation and comparison of Advanced Differential Interferometry Techniques: Murcia metropolitan area case study*, *ISPRS Journal of Photogrammetry and Remote Sensing*, **64**, pp. 501–512.
- Kersten, P.R., Lee, J.S. & Ainsworth, T.L. (2005), *A Comparison of Change Detection Statistics in POLSAR Images*, *Geoscience and Remote Sensing Symposium*, 2005. IGARSS '05. Proceedings. 2005 IEEE International , vol. **7**, no., pp. 4836–4839.
- Kratzsch, H. (Ed.) (1983), *Mining subsidence engineering*. Berlin: Springer-Verlag.
- Luo, H.M., Chen, E., Cheng, J. & Li, X. (2010), *Tree height retrieval methods using POLInSAR coherence optimization*, *Geoscience and Remote Sensing Symposium (IGARSS)*, IEEE International, pp. 3259–3262.
- Massonnet, D., Briole, P. & Arnaud, A. (1995), *Deflation of Mount Etna monitored by spaceborne radar interferometry*, *Nature*, **375**, pp. 567–570.
- Massonnet, D., Rossi, M., Carmona, C., Adragna, F., Peltzer, G., Feigl, K. & Rabaute, T. (1993), *The displacement field of the Landers earthquake mapped by radar interferometry*. *Nature*, **364**, pp. 138–142.
- Meng Liu; Hong Zhang; Chao Wang & Yixian Tang (2012), *Change detection of polarimetric SAR images applied to specific land cover type*, *Geoscience and Remote Sensing Symposium (IGARSS)*, 2012 IEEE International , pp. 6329–6332.
- Nguyen Ba Duy, Chatterjee R.S. & Vinay Kumar (2012), *Retrieval of PolSAR Decomposition Parameters Based Information for Land Use Land Cover* (2012), *Asia Pacific Conference on Environmental Science and Technology*, *Advances in Biomedical Engineering*, Vol. **6**.
- Poenaru, V., Badea, A. & Savin, E. (2012), *Assessment of the Ocnele Mari salt mine exploitation impacts on the Vegetation Coverage using multispectral remote sensing data*, *AgroLife Scientific Journal*, Vol. **1**, 2012, ISSN – 2285–5718.
- Poenaru, V., Dana, I., Teleagă, D., Poncos, V. (2013), *Land deformation monitoring in the Ocnele Mari salt mining area using VHR TSX data*, *TerraSAR-X Science Team Meeting*, 10–14 iunie 2013, DLR Oberpfaffenhofen, Germany.
- Poenaru, V.D., Badea, A., Savin, E., Teleaga, D. & Poncos, V. (2011), *Land degradation monitoring in the Ocnele Mari salt mining area using satellite imagery*, *Proceeding SPIE*, vol. 8181 818110U-1.
- Qi, Z., Yeh, Ago, Li, X. & Lin, Z. (2012), *A novel algorithm for land use and land cover classification using RADARSAT-2 polarimetric SAR data*, *Remote Sensing of Environment*, v. **118**, pp. 21–39.
- Qiang Chen; Gangyao Kuang; LI, J.; Lichun Sui & Diangang Li, *Unsupervised Land Cover/Land Use Classification Using PolSAR Imagery Based on Scattering Similarity*, *Geoscience and Remote Sensing, IEEE Transactions on* , vol. **51**, no. 3, pp. 1817–1825, March 2013 doi: 10.1109/TGRS.2012.2205389.

- Samieie-Esfahany, S., Hanssen, R., S., van Thienen-Visser, K. & Muntendam-Bos, A. (2009), *On the effect of horizontal deformation on InSAR subsidence estimates*, In: Proceeding of Fringe 2009 Workshop, ESA SP-677.
- Shuai Gao, Zheng Niu, Ni Huang & Xuehui Hou. (2013), *Estimating the leaf Area Index, height and biomass of maize using HJ-1 and Radarsat-2*, *International Journal of Applied Earth Observation and Geoinformation*, 24, <http://dx.doi.org/10.1016/j.jag.2013.02.002>
- Strozzi, T., & Wegmüller, U. (1999) *Land Subsidence in Mexico City Mapped by ERS Differential SAR Interferometry*, in Geoscience and Remote Sensing Symposium, 1999. IGARSS '99 Proceedings. IEEE 1999 International, vol. 4, pp. 1940–1942.
- Treuhaft, R.N. & Siqueira, P. (2000), *Vertical structure of vegetated land surfaces from interferometric and polarimetric radar*. *Radio Sci*, **35**, pp. 141–177.
- Trifu, C.I. & Shumila, V. (2010), *Microseismic Monitoring of a Controlled Collapse in Field II at Ocnele Mari, Romania*, *Pure Appl. Geophys.* **167** (2010), pp. 27–42.
- Werner, CL., Goldstein, R.M., Rosen, P. & Zebker, H.A. (1992), *Techniques and applications of SAR interferometry for ERS-1 topographic mapping, slope measurement and change detection*, Proceedings of the 1st Workshop ERS-1 FRINGE Working Group, ESA/ESRIN, pp. 11.
- Wright, T. J., Parsons, B. E. & Lu, Z. (2004), *Toward mapping surface deformation in three dimensions using InSAR*, *Geophys. Res. Lett.*, 31, L01607, doi:10.1029/2003GL018827.
- Yunjin Kim & van Zyl, J.J. (2009), *A Time-Series Approach to Estimate Soil Moisture Using Polarimetric Radar Data*," *Geoscience and Remote Sensing*, IEEE Transactions on, vol. **47**, no. 8, pp. 2519–2527.
- Zamfirescu, F., Giurgiu, N., Popescu, V. & Copaescu, S. (2010), *Present – day situation of Ocnele Mari wellfields following 48 years of the salt exploitation by dissolution already, close to be and approaching solved problems – a technical solution for the collapse fragmentation of the field 2 cavern Ocnele Mari, Romania*, Technical report.
- Zamfirescu, F., Mocuta, M., Constantinescu, T., Medves, E. & Danchiv, A. (2003), *The main causes of a geomechanical accident of brine caverns at field II of Ocnele Mari – Romania*, *Materials and geoenvironment*, Vol **50**, No. 1, pp. 431–434.
- Zebker, H. A. & Goldstein, R. M. (1986), *Topographic mapping from interferometric synthetic aperture radar observations*. *J. Geophys. Res.*, **91**(B5), pp. 4993–5000.
- Zebker, H.A. & Villasenor, J. (1992), *Decorrelation in interferometric radar echoes*, *IEEE Transactions on Geoscience and Remote Sensing*, Vol. **30**, pp. 950–959.

Received January 31, 2015